

Electrons and Phonons in YbC_6

I.I. Mazin

*Center for Computational Materials Science,
Naval Research Laboratory, Washington, DC 20375*

S.L. Molodtsov

Institut für Festkörperphysik, TU Dresden, D-01062 Dresden, Germany

(November 19, 2018)

The electronic structure and selected zone-center phonons in Yb graphite intercalation compound (YbC_6) are investigated theoretically using density functional calculations and LDA+U approximation for Coulomb correlations in the f shell, and experimentally using angle-resolved photoemission. We find that both in LDA and LDA+U approach the Yb f states are fully occupied providing no evidence for mixed-valent behavior. The obtained theoretical results are in good agreement with photoemission experiments. The $4f$ states are considerably hybridized both with the Yb $5d$ and C $2p$ states resulting in a substantial admixture of Yb f at the Fermi level. Soft Yb phonons, given a noticeable presence of the Yb states at the Fermi level, are probably responsible for the superconductivity recently reported in YbC_6 .

For a long time graphite intercalation compounds (GICs) have been attracting substantial attention due to their layered quasi-two dimensional (2D) structure and the resulting large anisotropy of their electric and electronic properties.^{1,2} Some of GICs are known to be superconducting at low temperatures.³ A renewed interest in superconducting phenomena in intercalated graphites is due to the recent discoveries of superconductivity in MgB_2 and B_xC , electronically related to graphite.⁴ An interesting example of graphite intercalation compounds is YbC_6 . First, it is one of the only four known bulk intercalations with $4f$ metals: YbC_6 , EuC_6 , SmC_6 , and TmC_6 ⁵ which may indicate that f electrons play certain role in bonding in these compounds. Likewise, YC_6 has not been synthesized so far, although Y behaves similar to lanthanides in systems with localized f electrons (cf. high- T_c cuprates). Last but not least, very recently superconductivity was discovered in YbC_6 .⁶

Yb is known to form mixed-valent compounds,⁷ so one may think mixed-valent physics is operative in YbC_6 as well. Therefore, it is of interest to investigate the electronic structure of YbC_6 numerically and experimentally. Should a good agreement between the theory and experiment be established, the former can be used to gain some insight into possible mechanism for superconductivity. Experimentally, Yb valence in the above compound can be obtained by recording the Yb $4f$ photoemission (PE) spectra. Due to the large Coulomb-correlation energy, the energy positions of the PE signals for $4f$ configurations with different electron occupations are shifted by several eV with respect to each other. Therefore, the contributions to the PE from different $4f$ configurations can easily be discriminated.⁸ From the intensity ratio of these contributions the information about the valence can be derived.

In this paper we present *ab initio* calculations of the

electronic structure of YbC_6 using both local density approximation (LDA) and LDA+U approach, which accounts for Coulomb correlations inside the f shell. The calculated energies for the Yb $4f$ states are in good agreement with the results of photoemission experiments giving no evidence for the mixed-valent behavior. We also report first principles calculations of selected zone center phonons. We find soft Yb-derived phonons to be likely responsible for the superconductivity reported in YbC_6 .

For the calculations, we used experimental crystal structure $P6/mmc$, with C occupying $12i$ and Yb $2d$ positions, with the lattice parameters $a = 4.32$ Å and $c = 9.1$ Å (Fig. 1). A full potential linear augmented plane wave method (LAPW) was used⁹ with the following setup: The APW sphere radii were taken as 2.5 and 1.3 bohr, the cutoff parameter $RK_{\max} = 7$, and local orbitals were used for Yb s and p and for C s , to reduce the linearization error, and to improve convergence in RK_{\max} . Linear tetrahedron method was employed for the Brillouin zone (BZ) integration, with the \mathbf{k} mesh up to $11 \times 11 \times 4$ divisions. Spin-orbit coupling was included on the second variational basis.⁹ The Ceperley-Alder exchange-correlation potential was used in the LDA part of the calculations. Finally, Hubbard correlations in the f shell were taken into account using the fully localized¹⁰ version of the LDA+U formalism, with the parameters $U = 0.4$ Ry and $J = 0.05$ Ry, estimated by modifying occupation numbers in the quasatomic loop in a LMTO (linear muffin-tin orbital) program.

The Yb-GIC samples for the PE experiments were prepared *in situ* by thermally driven surface reaction of deposited Yb overlayers with graphite (0001) substrate as described elsewhere.¹¹ The measurements were performed using synchrotron radiation from various beamlines at BESSY/Berlin electron storage ring. Angle-resolved photoemission spectra (ARPES) were taken

with 33 eV photon energy using rotative hemispherical electron energy analyzers (VSW-ARIES) tuned to an energy resolution 150 meV (full width at half maximum, FWHM) and an angular resolution of 1°. Basic pressure during measurements was always better than 1×10^{-10} mbar.

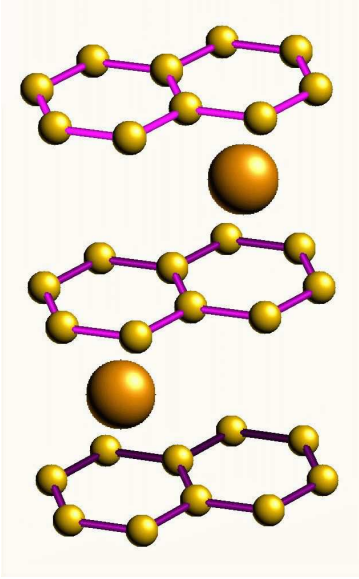


FIG. 1. Crystal structure of YbC_6 . Large spheres denote Yb and small spheres denote C. (color online)

The band structure calculated within the LDA+U scheme is shown in Fig. 2. Probably the most intriguing observation is that all f states appear to be fully occupied, giving evidence to firmly divalent Yb. This seems to be related to the fact that straight LDA calculation (not shown), without any account of intra- f -shell Hubbard-type correlations, still place all f bands below the Fermi level, although, of course, much higher in energy than in LDA+U.

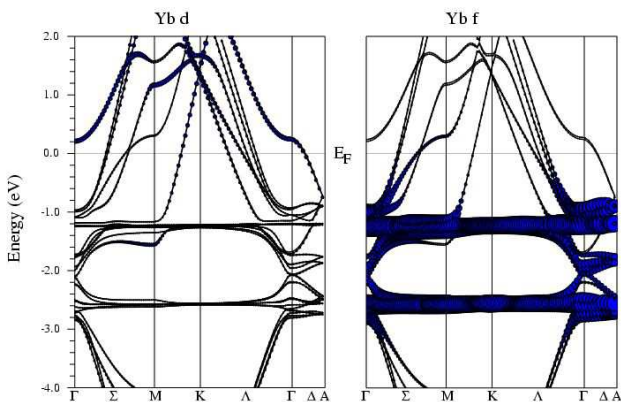


FIG. 2. LDA+U band structure of YbC_6 . The left panel shows the partial Yb- d character, and the right panel Yb- f character. (color online)

The spin-orbit interaction splits the f states into two manifolds, located 1.10 and 2.30 eV below the Fermi level (E_F). The corresponding total electronic density of states (DOS) with two strong peaks originating in the $4f$ states is demonstrated in Fig. 3. Calculated positions of the $4f$ states in lanthanide systems depend very much on specific choice of U and J values, which are often used as fitting parameters to achieve better correspondence with the experimental data. It is very important to note that in the present study the U and J values were estimated from the first principles and no attempts were done to fit or tune this parameters.

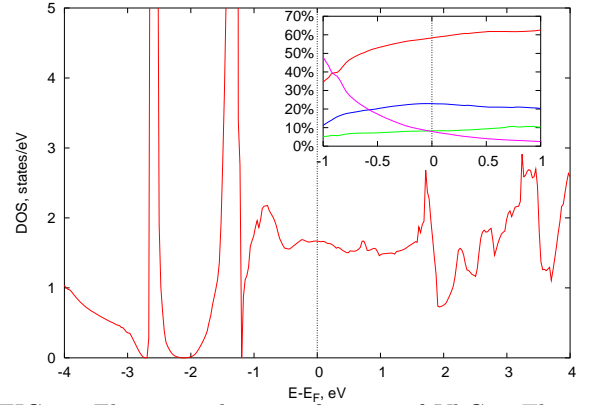


FIG. 3. Electronic density of states of YbC_6 . The main graph shows the total DOS on a per-formula-unit basis and the insert shows, in the order from the lowest to highest DOS at $E - E_F = 1$ eV, the partial contribution of Yb f , Yb d , C p character inside the corresponding APW spheres and the contribution of interstitial states. (color online)

Most importantly, the qualitative prediction of purely divalent Yb in Yb-GIC is unambiguously supported by the PE data. Fig. 4 depicts a series of angle-resolved PE spectra taken along the Γ - K' - M' direction in the BZ of graphite. All four characteristic occupied bands of graphite (σ_{1v} , σ_{2v} , σ_{3v} , and π_{1v}) are clearly seen in the figure pointing to the high-quality intercalation compound under consideration.¹¹ The Fermi-energy peak appearing in the region close to the K' point stems from the bottom of the π_0^* band of graphite, which becomes occupied in the GIC due to charge transfer of electrons from the intercalant atoms. The none-dispersive divalent contributions into the PE signal of the Yb $4f$ electrons, which are found at 1.14 eV and 2.41 eV binding energies (BEs), are marked by two thin lines through the spectra. Would the divalent $4f$ component of the final-state PE multiplet be observed at the Fermi energy, it will show that the final-state multiplet is energetically degenerate with the ground state that will provide a reason for homogeneous mixed-valent behavior of the system. In the present case of the Yb-GIC, the divalent signal is observed too far from E_F to anticipate the mixed-valent properties of the compound. Correspondingly, no traces of a trivalent signal in the region of 5 to 12 eV BE,⁸ which

one would expect for a mixed-valent system, are seen in the photoemission spectra.

The experimentally obtained binding energies of the divalent $4f$ contributions are in excellent agreement with the theoretical values. Not only energies, but also line-shapes of the DOS and PE spectra are in agreement with each other. In the right panel of Fig. 4 we compare the angle-resolved PE spectrum sampling electronic states in the region of the M point in the BZ of the Yb-GIC with the local DOS (spectral function) calculated around this point. The calculated local DOS was broadened with a Lorentzian to account for finite lifetime effects. Good correspondence between the theoretical and experimental data is evident in the figure. In fact, the agreement is better than one expects given the approximations used. Nevertheless, even though such level of accuracy is likely fortuitous, this clearly indicates that the underlying physics is correctly described by the calculations, and, importantly, that the derived value of U and J are in the right ballpark.

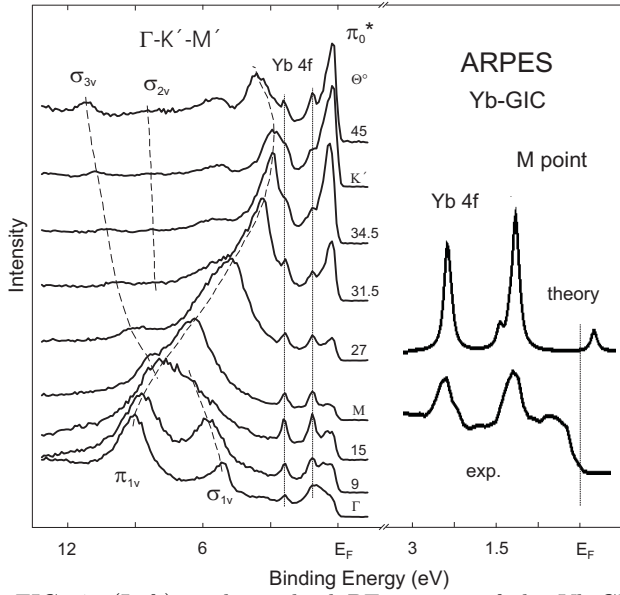


FIG. 4. (Left) angle-resolved PE spectra of the Yb-GIC taken along the Γ - K' - M' direction in the BZ of graphite (Γ - M - Γ - M in the BZ of the Yb-GIC) at different polar angles Θ . (Right) Comparison between the local DOS in the vicinity of the M point and the angle-resolved PE spectrum sampling this region.

We shall now discuss the calculated electronic structure in more detail. Even in the vicinity of the Fermi level, the bands of YbC_6 are qualitatively different from that of YC_6 (Fig. 2), indicating that the hybridization of the f states with the itinerant electrons should play an important role in transport properties in this material. There are 12 bands crossing the Fermi level. However, spin-orbit splitting at E_F is very small, so that one can safely speak about 6 distinct Fermi surfaces, corresponding to bands 1, 3, 5, 7, 9, and 11, shown in Fig. 5. An

easy way to make the correspondence between the Fermi surfaces and the bands plotted in Fig. 2 is to count them from K to Γ : the only band crossing the Fermi level between K and M is band 1(2), while the state at approximately 0.2 eV at Γ is band 11(12). Bands 1, 5, 7, and 9 are quasi 2D, while bands 3 and 11 have considerable dispersion along the z direction. It is instructive to look at the element specific character of these bands. Band 11, forming elliptical pockets around Γ , has more Yb character than C, and namely $\text{Yb } d_{z^2-r^2}$ character. Not surprisingly, this is the band that is most dispersive in the z direction. Bands 5 through 8 have predominantly C p_z origin (band 5 with a considerable hybridization with Yb f), while bands 1 and 3 show only small contributions within either C or Yb muffin-tin spheres, but rather in the interstitial areas, thus being mostly free-electron like.

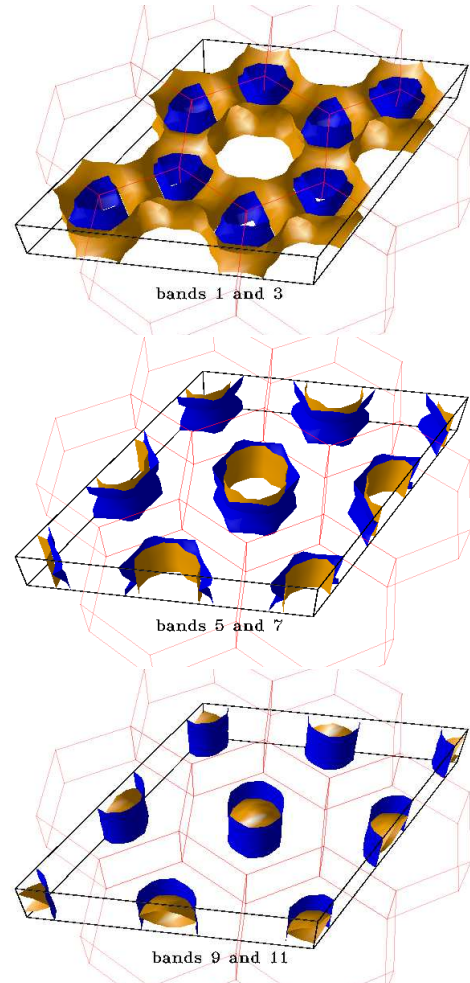


FIG. 5. LDA+U Fermi surface of YbC_6 . The band with the lower index is blue (darker in grey scale). (color online)

While at the Fermi level most of the DOS (inset in Fig. 3) comes from the extended states in the interstitial region, there is a noticeable share of the Yb f states, which rapidly grows with increasing BE. Contribution of the Yb d states (mostly $d_{z^2-r^2}$ symmetry) is

also considerable. This indicates that (i) Yb phonons may play a role in superconductivity and (ii) substituting Yb by other divalent elements, like Ca, may change superconducting properties substantially, or destroy superconductivity at all. The total density of states at the Fermi level is $N(E_F) = 1.7$ states/(eV·formula). The average Fermi velocity in- and out-of-plane, respectively, is 4.8×10^7 and 2.7×10^7 cm/sec. The corresponding components of the plasma frequency are 6.2 and 3.6 eV, implying, in the constant scattering rate approximation, a resistivity anisotropy of about 3.

The large unit cell of YbC_6 allows for multiple zone-center modes, which in principle can be computed by the frozen phonon method. 24 modes corresponding to in-plane motion of C are expected to be very hard, since C $p_{x,y}$ orbitals are removed from the Fermi level (as opposed, for instance, to MgB_2). Indeed, we calculated the frequency of the fully symmetric A_{1g} mode to be 1540 cm $^{-1}$. Most of the 12 out-of-plane C modes, by symmetry, have zero deformation potential at Γ and thus do not couple with electrons, while the E_g mode lowers the symmetry to triclinic and is prohibitively difficult to compute accurately. Thus, we are left with the 6 Yb modes, of which the three even modes correspond to a double degenerate E_{2g} phonon involving displacements of Yb parallel to the graphite plane, and a B_{1g} one, corresponding to Yb displacements along c . These modes are rather soft; our calculations place them at 77 and 153 cm $^{-1}$, respectively. Unfortunately, the electron-phonon coupling exactly at the zone center is strongly suppressed by symmetry for these three modes (if the alternating Yb planes were not shifted with respect to each other, cf. Fig. 1, it would be forbidden, so in the actual structure it is suppressed to the extent of the weakness of Yb-Yb interaction. However, their low frequency and considerable presence of Yb character at the Fermi level suggest that coupling of these and similar modes, when integrated over the Brillouin zone, may be sufficient to explain superconductivity in YbC_6 .

Work at the Naval Research Laboratory was supported by the Office of the Naval Research. Experimental part was supported by the Deutsche Forschungsgemeinschaft, SFB 463 (TP B16).

¹ *Intercalation Compounds of Graphite*, ed. by F.L. Fogel and A. Herold (Elsevier Sequoia, Lausanne, 1977).

² *Intercalation in Layered Materials*, ed. by M.S. Dresselhaus, NATO ASI Series B: Physics Vol. 148 (Plenum Press, New York, 1986).

³ N.B. Hannay, T.H. Geballe, B.T. Matthias, K. Andres, P. Schmidt, and D. MacNair, *Phys. Rev. Lett.* **14**, 225 (1965).

⁴ I.I. Mazin and V.P. Antropov, *Physica C* **385**, 49 (2003).

⁵ M. El Makrini, D. Guérard, P. Lagrange, A. Hérol, *Physica B* **99**, 481 (1980); M.S. Dresselhaus and G. Dresselhaus, *Adv. in Phys.* **30**, 139 (1981).

⁶ M. Ellerby *et al.*, unpublished (reported at the Gordon Conference on Superconductivity, Oxford, 2004).

⁷ *Valence Fluctuations in Solids*, ed. by L.M. Falicov, W. Hanke and M.B. Maple (North-Holland, Amsterdam, 1981).

⁸ S. Wieling, S.L. Molodtsov, Th. Gantz, J.J. Hinarejos, C. Laubschat, and M. Richter, *Phys. Rev. B* **58**, 13219 (1998); S. Wieling, S.L. Molodtsov, Th. Gantz, and C. Laubschat, *Phys. Rev. B* **64**, 125424 (2001).

⁹ P. Blaha, K. Schwarz, G.K.H. Madsen, D. Kvasnicka, and J. Luitz, *Wien*, 2002, an Augmented Plane Wave + Local Orbitals Program for Calculating Crystal Properties (Karlheinz Schwarz, Techn. Universität Wien, Austria) ISBN 3-9501031-1-2.

¹⁰ A.G. Petukhov, I.I. Mazin, L. Chioncel, and A.I. Lichtenstein, *Phys. Rev. B* **67**, 153106 (2003).

¹¹ S.L. Molodtsov, Th. Gantz, C. Laubschat, A.G. Viatkine, J. Avila, C. Casado, and M.C. Asensio, *Z. Phys. B* **100**, 381 (1995); S.L. Molodtsov, C. Laubschat, M. Richter, Th. Gantz, and A.M. Shikin, *Phys. Rev. B* **53**, 16621 (1996).